ChemComm
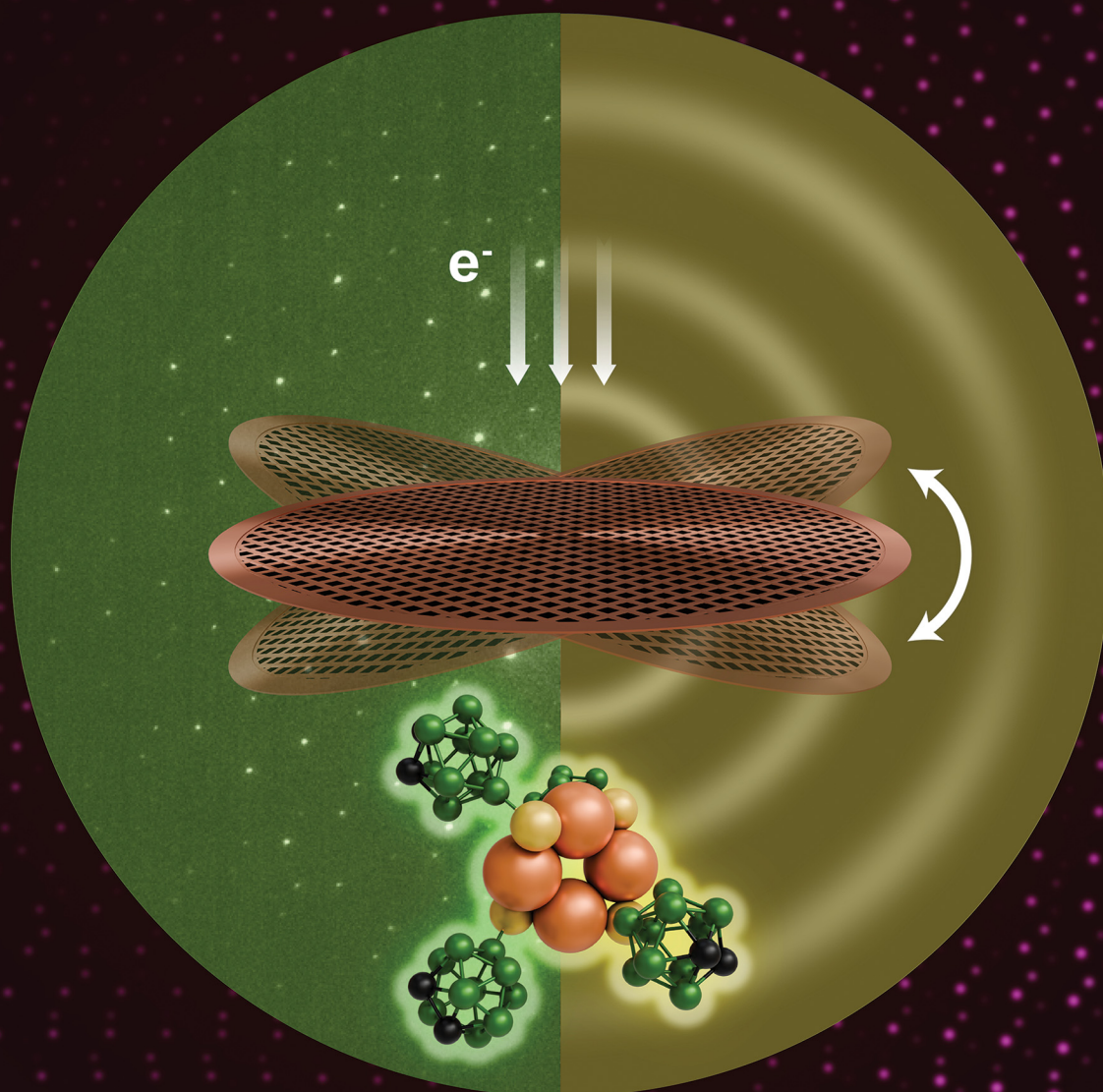
Chemical Communications

rsc.li/chemcomm

COMMUNICATION

Tomas Base, Anirban Som, Brent L. Nannenga,
Thalappil Pradeep *et al.*
Mechanochromic luminescence in copper nanoclusters:
resolving structural transitions through microcrystal electron
diffraction

ROYAL SOCIETY
OF **CHEMISTRY**

Mechanochromic luminescence in copper nanoclusters: resolving structural transitions through microcrystal electron diffraction†‡

Harshita Nagar, [ab] Subrata Duary,[ab] Vivek Yadav,[ab]
Amoghavarsha Ramachandra Kini,[ab] Sudhadevi Antharjanam,[c] Tomas Base, [*d]
Anirban Som, [*ab] Brent L. Nannenga [*e] and Thalappil Pradeep [*ab]

MicroED reveals insights into mechanochromic luminescence in copper nanoclusters, demonstrating structural transitions from crystalline to amorphous state upon grinding, with restoration of crystallinity following solvent exposure. Luminescence switching occurs due to reversible amorphization-recrystallization rather than chemical changes, providing critical design principles for such stimuli-responsive materials.

Noble metal nanoclusters (NCs) occupy a unique position between atomic and nanoparticle regimes of matter, exhibiting quantum-confined properties that depend critically on their precise atomic arrangements.[1,2] Accurate structural insight enables the building of structure–property relationships, identification of active sites for catalysis,[3] optimization of functionalities,[4] and doping of heteroatoms[5,6] for various applications in energy, medicine, and nanotechnology.[7–9] Detailed structural information also helps to understand stability, growth mechanisms, and ligand–cluster and cluster–cluster interactions, which are essential for tailoring the performance of NCs.[10] Among NCs, copper nanoclusters (Cu NCs) have emerged as useful materials due to their mechanochromic luminescence[11–13] and reversible emission changes upon mechanical grinding and solvent exposure, making them promising for sensing and *anti*-counterfeiting applications. Despite their emerging importance, the structural mechanisms underlying

reversible luminescence remain poorly understood, primarily due to analytical limitations.

Conventional structural methods face significant challenges when investigating mechanochromic transitions. Single-crystal X-ray diffraction (SC-XRD), gold-standard for structure determination, fails when crystal size reduces to submicron dimensions after mechanical processing, while powder XRD provides limited atomic-level detail. This analytical gap has hindered mechanistic understanding of how grinding-induced structural changes correlate with altered luminescence properties, leaving fundamental questions about structural integrity and solvent interactions unresolved.

Microcrystal electron diffraction (MicroED) addresses these limitations by enabling atomic-resolution structure determination from submicron-sized crystals.[14] While used extensively for biomolecules[15] and previously applied to a single gold NC,[16] MicroED's potential for investigating mechanochromic phenomena in NCs remain unexplored. This technique is particularly suited for studying Cu NCs' complex behaviors given their distinctive coordination chemistry and cuprophilic interactions that fundamentally influence their photoluminescent properties.

Here, we demonstrate MicroED's capabilities through progressive investigation of three 4-atom Cu NC systems: first showcasing its accuracy through structural analysis of $Cu_4(MNA)_2(DPPE)_2$, then revealing solvent molecules in $Cu_4(m_9\text{-}CBT)_4$ undetectable by SC-XRD, and finally providing direct structural evidence of the amorphization-recrystallization mechanism in mechanochromic $Cu_4(o_9\text{-}CBT)_4$ (MNA, DPPE, o_9-CBT and m_9-CBT are 2-mercaptonicotonic acid, 1,2-bis-(diphenylphosphino) ethane, *ortho* carborane-9-thiol and *meta* carborane-9-thiol, respectively). Our findings establish that mechanical grinding disrupts long-range order without altering the structure of individual NCs, while solvent exposure facilitates recrystallization and restoration of luminescence, insights previously inaccessible through conventional techniques.

Previously reported by our group, these three Cu NCs serve as ideal candidates for MicroED investigations, exhibiting assembly-induced emission wherein their non-emissive solution behavior transforms to bright solid-state luminescence through molecular

a DST Unit of Nanoscience (DST UNS) and Thematic Unit of Excellence (TUE), Department of Chemistry, Indian Institute of Technology, Madras, Chennai – 600036, India. E-mail: pradeep@iitm.ac.in, asomchem@gmail.com

b International Centre for Clean Water, Chennai-600113, India

c Sophisticated Analytical Instruments Facility (SAIF), Indian Institute of Technology, Madras, Chennai – 600036, India

d Department of Synthesis, Institute of Inorganic Chemistry, The Czech Academy of Science, 1001 Husinec-Rez, 25068, Czech Republic. E-mail: tbase@iic.acs.cz

e School of Engineering of Matter, Transport and Energy, Arizona State University, Tempe, Arizona, USA. E-mail: brent.nannenga@asu.edu

† Dedicated to Prof. C. N. R. Rao, FRS on his 91st birthday.

‡ Electronic supplementary information (ESI) available. See DOI: https://doi.org/10.1039/d5cc02594j

ordering.[17,18] Their distinctive mechanochromic response provides a perfect platform for elucidating structure–property relationships at the nanoscale. The synthesis and crystallization protocols for these NCs are described in the Experimental section (ESI‡). These were fully characterized using UV-vis spectroscopy and ESI-MS (Fig. S1, ESI‡). For MicroED, microcrystals were deposited onto lacey carbon grids, clipped into autogrid-rings, and loaded into a Krios G4 Cryo-EM equipped with an X-FEG source operating at 300 kV (Fig. S2, ESI‡). Data were collected using EPU-D (ThermoFisher), with the overall procedure illustrated in Fig. S3 (ESI‡). An atlas preset at low magnification provided a global map, followed by a grid square preset to image a single region, then a search/auto eucentric preset to locate and center the crystals of interest, and finally a diffraction preset for the collection of continuous rotation electron diffraction data at a dose rate of 0.01 e$^-$ Å^{-2} s^{-1} using the smallest spot size (11) and a 1 s exposure, in nanoprobe mode. Samples were maintained at liquid nitrogen temperature, and diffraction data were recorded on a Ceta D CMOS camera and exported in SMV format. All diffraction datasets were indexed and integrated using XDS, scaled with XSCALE, and then converted to SHELX format through XDSCONV. Structures were subsequently solved with SHELXT and refined in SHELXL. Notably, the entire MicroED data collection and structure determination process required only a few hours, underscoring the rapid and efficient nature of this technique.

We first investigated Cu$_4$(MNA)$_2$(DPPE)$_2$ NC as a benchmark system to validate MicroED's capability for accurate structure determination of copper clusters. Microcrystals (Fig. 1A) suspended in DMF were deposited directly onto lacey carbon grids and analyzed using the continuous rotation methodology. Data collection from $-50°$ to $+50°$ in $1°$ increments at $1°$ s^{-1} achieved exceptional subatomic resolution (0.8 Å, Fig. 1B), comparable to high-quality SC-XRD data but from significantly smaller crystals. TEM images of the microcrystal at various tilt angles are shown in Fig. S4 (ESI‡).

The resulting structure revealed a Cu$_4$S$_2$ core formed by two Cu$_2$ units connected through bridging sulfur atoms (Fig. 1C). Each Cu$_2$ unit exhibited distinctive coordination environments:
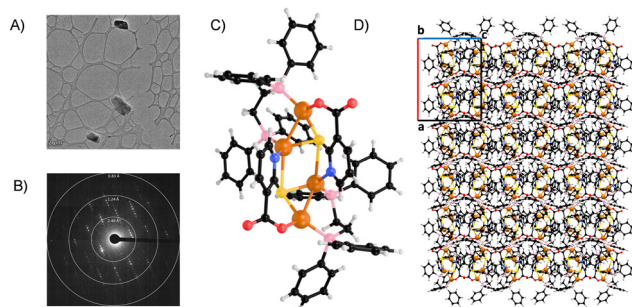
one copper center adopted tetrahedral coordination (μ_3-S, P, O, and Cu), while the other displayed pentacoordination (two μ_3-S, P, N, and Cu). This arrangement suggests cuprophilic interactions between copper centers. The DPPE ligands coordinated through phosphorus, while MNA was bound via nitrogen and oxygen atoms, creating a stable structural framework. Packing of the structure ($3 \times 3 \times 3$ along the b-axis) is shown in Fig. 1D and unit cell molecular packing along different axes are shown in Fig. S5 (ESI‡). Notably, all the geometric parameters determined through MicroED, including bond lengths, angles, and intermolecular distances matched well with the SC-XRD data (Table S1, ESI‡) validating MicroED's reliability for Cu NC characterization. These findings match perfectly with the SC-XRD structure (Fig. S6 ESI‡).

Building upon the successful structure determination of Cu$_4$(MNA)$_2$(DPPE)$_2$, we next examined Cu$_4$(m_9-CBT)$_4$, where MicroED revealed critical structural insights beyond those accessible through conventional methods. Gently crushed crystals deposited on lacey carbon grids (Fig. 2A) were analyzed using MicroED with $1°$ continuous tilt increments over a $-40°$ to $+40°$ rotation range, achieving 0.9 Å resolution (Fig. 2B). The most significant finding was the detection of a disordered toluene (solvent) molecule within the unit cell (Fig. 2C), a critical structural feature not observed from SC-XRD (Fig. S7, ESI‡). This discovery necessitated reassignment of the space group from $P2_1/c$ (SC-XRD) to $P\bar{1}$ (MicroED), with corresponding adjustments to cell parameters (Table S2, ESI‡). MicroED-derived packing ($3 \times 3 \times 3$ along the c-axis) is shown in Fig. 2D and views along different axes are shown in (Fig. S8, ESI‡). The stronger interaction of electrons with matter makes MicroED particularly sensitive to lighter atoms and disordered structures, providing a more complete picture of the molecular environment within the crystal lattice. This finding highlights a
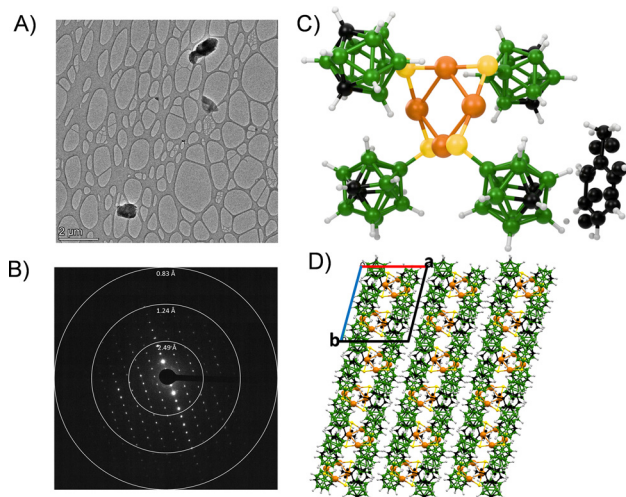

Fig. 1 MicroED enables subatomic resolution structure determination of Cu$_4$(MNA)$_2$(DPPE)$_2$. (A) TEM image of microcrystals on lacey carbon grids. (B) Initial diffraction frame showing high resolution reflections. (C) Resolved molecular structure revealing Cu$_4$S$_2$ core with distinct coordination environments. (D) $3 \times 3 \times 3$ crystal packing along b-axis. Color code: Cu (orange), S (yellow), O (red), N (blue), P (pink), C (black), H (white).

Fig. 2 MicroED reveals solvent inclusion in the Cu$_4$(m_9-CBT)$_4$ structure. (A) TEM image of microcrystals. (B) Initial diffraction frames showing high-resolution data. (C) Resolved structure highlighting the disordered toluene molecule undetectable by SC-XRD. (D) $3 \times 3 \times 3$ crystal packing along c-axis. Color code: Cu (orange), S (yellow), B (green), C (black), H (white).

distinctive advantage of MicroED: its capacity to resolve subtle structural features that might be missed by SC-XRD. It is important to note that geometric parameters observed through MicroED in the individual clusters were largely similar to that known from SC-XRD.

Previous studies on copper clusters have demonstrated that solvent molecules can modify intermolecular interactions and affect emission properties.[19] Perruchas *et al.* observed that changes in crystal packing and cuprophilic interactions directly influence luminescence behavior.[13] The ability to detect these previously invisible structural elements provides crucial insights into structure–property relationships in luminescent copper clusters.

This enhanced structural information proves valuable for understanding the factors that influence luminescence properties and mechanochromic behavior, which were explored further. The $Cu_4(o_9\text{-}CBT)_4$ cluster exhibits a shift in emission from green to yellow upon mechanical grinding (~ 20 min), with restoration of the original emission following exposure to solvent vapor (DCM, ~ 30 min),[18] shown in Fig. 3A. Similar mechanochromic luminescence has been observed in various copper complexes, particularly copper iodide clusters with cubane geometry $[Cu_4I_4L_4]$.[13] However, the underlying structural mechanism has remained elusive due to the inability to

obtain high-quality diffraction data from mechanically processed materials.

We conducted systematic MicroED analysis at three critical stages: before grinding, after grinding, and following solvent vapor exposure. The diffraction patterns clearly demonstrated: (i) well-defined crystallinity in the initial state, (ii) complete loss of diffraction following prolonged grinding, indicating amorphization, and (iii) restored crystallinity upon solvent vapor exposure (Fig. 3B). High-quality diffraction data enabled sub-atomic resolution (0.9 Å) structure determination (Fig. 3C) of the NC. Most remarkably, MicroED successfully resolved the structure from nanometer-sized regrown crystals after solvent exposure, confirming restoration of the original structural arrangement (Fig. 3E). The ground powder yielded no structure due to unresolvable diffraction (Fig. 3D).

This observation aligns with previous studies of copper iodide clusters, where mechanochromic properties have been attributed to distortions in crystal packing affecting cuprophilic interactions. As reported by Perruchas *et al.*, grinding-induced structural disorder can modify Cu–Cu interactions without altering the fundamental molecular structure, directly influencing emission properties.[20] The structural insights from our observations find strong theoretical support in the mechanochemical principles outlined by Yan *et al.* in their work on
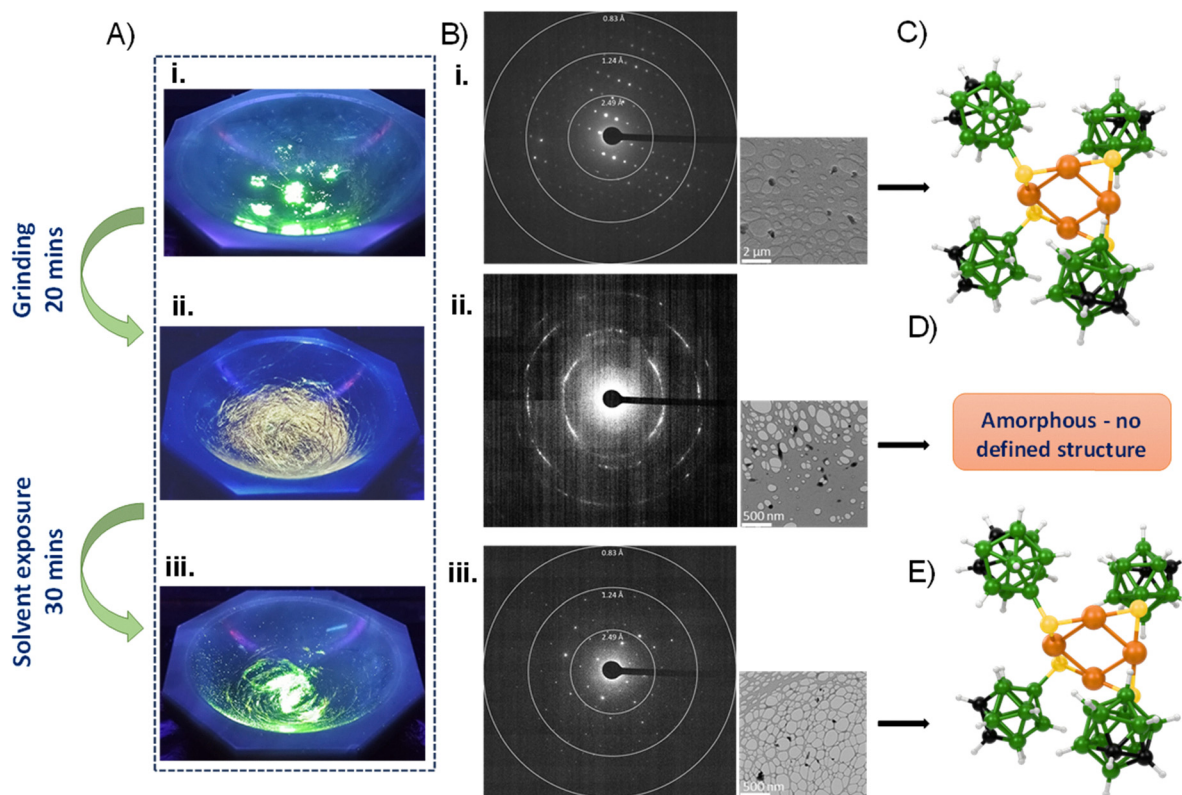

Fig. 3 MicroED directly visualizes the structural basis of mechanochromic luminescence in $Cu_4(o_9\text{-}CBT)_4$. (A) Photographic images demonstrating reversible emission switching: (i) initial green emission, (ii) yellow emission after grinding (20 min), and (iii) restored green emission following DCM vapor exposure (30 min). (B) Corresponding diffraction patterns revealing: (i) initial crystallinity, (ii) complete amorphization after grinding, and (iii) restored crystallinity after solvent exposure. Crystallite sizes are visible in the inset TEM images. (C) MicroED structure from initial crystalline state. (D) Amorphous state with no resolvable structure after grinding. (E) Recovered structure from nanometer-sized recrystallized particles after solvent exposure, confirming structural restoration without molecular alteration.

sterically controlled reactions under hydrostatic pressure.[21] Their demonstration that isotropic compression induces anisotropic strain in metal–organic chalcogenides, particularly through ligand-mediated deformation of compressible Cu_4S_4 cores (Fig. S9, ESI‡) directly parallels our observation of amorphization-recrystallization cycles in $Cu_4(o_9\text{-CBT})_4$. They showed that rigid ligands (carboranes) act as "molecular anvils", transmitting stress to bend Cu–S–Cu bond angles. This aligns with our findings that grinding-induced loss of long-range order without Cu–S bond rupture drives luminescence switching, while solvent exposure enables structural recovery through ligand reorganization. Our direct structural evidence confirms that mechanochromic luminescence in $Cu_4(o_9\text{-CBT})_4$ arises from disruption of long-range order followed by recrystallization, rather than chemical transformation or degradation. Fig. S10 (ESI‡) displays unit cell packing of $Cu_4(o_9\text{-CBT})_4$ in both initial crystalline state and after solvent-induced recrystallization along various axes. Comparative analysis of geometric parameters like bond lengths, angles, and intermolecular distances, from structures before grinding and after solvent vapor exposure showed remarkable consistency (Table S3, ESI‡). This confirms that individual Cu NCs maintain their molecular integrity throughout the mechanochromic cycle, with changes occurring primarily in their arrangement and long-range order. The emission shift correlates directly with the loss of crystallinity, while recovery of the original emission coincides with recrystallization.

In conclusion, the ability to directly observe this relationship through MicroED analysis of submicron crystallites provides unprecedented insights into the structure–property relationship underlying mechanochromic behavior. Unlike previous studies that relied on indirect spectroscopic evidence or theoretical calculations, our approach provides direct structural confirmation of the mechanochromic mechanism. This represents a significant advancement in understanding stimuli-responsive luminescent materials and demonstrates MicroED's exceptional utility for studying mechanical transformations of functional materials.

Conflicts of interest

There are no conflicts to declare.

Data availability

The data supporting this article have been included in the ESI.‡

Notes and references

1 I. Chakraborty and T. Pradeep, *Chem. Rev.*, 2017, **117**, 8208–8271.
2 R. Jin, C. Zeng, M. Zhou and Y. Chen, *Chem. Rev.*, 2016, **116**, 10346–10413.
3 Y. Du, H. Sheng, D. Astruc and M. Zhu, *Chem. Rev.*, 2020, **120**, 526–622.
4 Nonappa, *Chem. Commun.*, 2023, **59**, 13800–13819.
5 S. Hossain, Y. Niihori, L. V. Nair, B. Kumar, W. Kurashige and Y. Negishi, *Acc. Chem. Res.*, 2018, **51**, 3114–3124.
6 A. Ghosh, O. F. Mohammed and O. M. Bakr, *Acc. Chem. Res.*, 2018, **51**, 3094–3103.
7 M. F. Matus and H. Häkkinen, *Nat. Rev. Mater.*, 2023, **8**, 372–389.
8 K. S. Sugi, A. Maier and M. Scheele, *Chem. Commun.*, 2022, **58**, 6998–7017.
9 Y. Tao, M. Li, J. Ren and X. Qu, *Chem. Soc. Rev.*, 2015, **44**, 8636–8663.
10 K. R. Krishnadas, A. Ghosh, A. Baksi, I. Chakraborty, G. Natarajan and T. Pradeep, *J. Am. Chem. Soc.*, 2016, **138**, 140–148.
11 A. Baghdasaryan and T. Bürgi, *Nanoscale*, 2021, **13**, 6283–6340.
12 A. Ghosh, A. Sagadevan, K. Murugesan, S. A. F. Nastase, B. Maity, M. Bodiuzzaman, A. Shkurenko, M. N. Hedhili, J. Yin, O. F. Mohammed, M. Eddaoudi, L. Cavallo, M. Rueping and O. M. Bakr, *Mater. Horiz.*, 2024, **11**, 2494–2505.
13 Q. Benito, X. F. Le Goff, S. Maron, A. Fargues, A. Garcia, C. Martineau, F. Taulelle, S. Kahlal, T. Gacoin, J.-P. Boilot and S. Perruchas, *J. Am. Chem. Soc.*, 2014, **136**, 11311–11320.
14 B. L. Nannenga and T. Gonen, *Curr. Opin. Struct. Biol.*, 2014, **27**, 24–31.
15 X. Mu, C. Gillman, C. Nguyen and T. Gonen, *Annu. Rev. Biochem.*, 2021, **90**, 431–450.
16 S. Vergara, D. A. Lukes, M. W. Martynowycz, U. Santiago, G. Plascencia-Villa, S. C. Weiss, M. J. De La Cruz, D. M. Black, M. M. Alvarez, X. López-Lozano, C. O. Barnes, G. Lin, H.-C. Weissker, R. L. Whetten, T. Gonen, M. J. Yacaman and G. Calero, *J. Phys. Chem. Lett.*, 2017, **8**, 5523–5530.
17 S. Duary, A. Jana, A. Das, S. Acharya, A. R. Kini, J. Roy, A. K. Poonia, D. K. Patel, V. Yadav, P. K. S. Antharjanam, B. Pathak, A. Kumaran Nair Valsala Devi and T. Pradeep, *Inorg. Chem.*, 2024, **63**, 18727–18737.
18 A. Jana, M. Jash, W. Ahmed Dar, J. Roy, P. Chakraborty, G. Paramasivam, S. Lebedkin, K. Kirakci, S. Manna, S. Antharjanam, J. Machacek, M. Kucerakova, S. Ghosh, K. Lang, M. M. Kappes, T. Base and T. Pradeep, *Chem. Sci.*, 2023, **14**, 1613–1626.
19 A. Jana, S. Duary, A. Das, A. R. Kini, S. Acharya, J. Machacek, B. Pathak, T. Base and T. Pradeep, *Chem. Sci.*, 2024, **15**, 13741–13752.
20 S. Perruchas, X. F. Le Goff, S. Maron, I. Maurin, F. Guillen, A. Garcia, T. Gacoin and J.-P. Boilot, *J. Am. Chem. Soc.*, 2010, **132**, 10967–10969.
21 H. Yan, F. Yang, D. Pan, Y. Lin, J. N. Hohman, D. Solis-Ibarra, F. H. Li, J. E. P. Dahl, R. M. K. Carlson, B. A. Tkachenko, A. A. Fokin, P. R. Schreiner, G. Galli, W. L. Mao, Z.-X. Shen and N. A. Melosh, *Nature*, 2018, **554**, 505–510.